HHS Public Access

Author manuscript

Cancer Immunol Res. Author manuscript; available in PMC 2024 March 01.

Published in final edited form as:

Cancer Immunol Res. 2023 September 01; 11(9): 1222–1236. doi:10.1158/2326-6066.CIR-22-0254.

AXL inhibition improves the anti-tumor activity of chimeric antigen receptor T cells

R. Leo Sakemura[1,2], **Mehrdad Hefazi**[1,2], **Michelle J. Cox**[1], **Elizabeth L. Siegler**[1,2], **Sutapa Sinha**[2], **Michael J. Hansen**[3], **Carli M. Stewart**[1,2,4,5], **Jennifer M. Feigin**[1], **Claudia Manriquez Roman**[1,2,4,6], **Kendall J. Schick**[1], **Ismail Can**[1,2], **Erin E. Tapper**[1], **Paulina Horvei**[1], **Mohamad M. Adada**[1,2], **Evandro D. Bezerra**[1], **Lionel Aurelien Kankeu Fonkoua**[1,2], **Michael W. Ruff**[1,7], **Cynthia L. Forsman**[1], **Wendy K. Nevala**[3], **Justin C. Boysen**[2], **Renee C. Tschumper**[3], **Cory L. Grand**[8], **Kameswara R. Kuchimanchi**[8], **Lars Mouritsen**[8], **Jason M. Foulks**[8], **Steven L. Warner**[8], **Timothy G. Call**[2], **Sameer A. Parikh**[2], **Wei Ding**[2], **Neil E. Kay**[2], **Saad S. Kenderian**[1,2,3,6]

[1]T Cell Engineering, Mayo Clinic, Rochester, MN, USA

[2]Division of Hematology, Mayo Clinic, Rochester, MN, USA

[3]Department of Immunology, Mayo Clinic, Rochester, MN, USA

[4]Mayo Clinic Graduate School of Biomedical Sciences, Rochester, MN, USA

[5]Department of Molecular Pharmacology & Experimental Therapeutics, Mayo Clinic, Rochester, MN, USA

[6]Department of Molecular Medicine, Mayo Clinic, Rochester, MN, USA

[7]Department of Neurology, Mayo Clinic, Rochester, MN, USA

[8]Sumitomo Dainippon Pharma Oncology, Inc. Lehi, UT, USA

Abstract

The receptor tyrosine kinase AXL is a member of the TAM (Tyro3, AXL, and proto-oncogene tyrosine-protein kinase Mer) family and plays pleiotropic roles in cancer progression. AXL is expressed in immunosuppressive cells, which contributes to decreased efficacy of immunotherapy. Therefore, we hypothesized that AXL inhibition could serve as a strategy to overcome resistance to chimeric antigen receptor T (CART)-cell therapy. To test this, we determined the impact of AXL inhibition on CD19-targeted CART (CART19)-cell functions. Our results demonstrate that T cells and CART cells express high levels of AXL. Specifically, higher levels of AXL on activated Th2 CART cells and M2-polarized macrophages were observed. AXL inhibition with small molecules or via genetic disruption in T cells demonstrated selective inhibition of Th2 CART cells, Th2 cytokines, reversal of CART-cell inhibition, and promotion of CART-cell

Corresponding author: Saad S. Kenderian, M.D, Assistant Professor of Medicine, Oncology and Immunology, Mayo Clinic College of Medicine, 200 First Street SW, Rochester, MN 55905, Tel (507) 284-2511, Kenderian.saad@mayo.edu.

AUTHORSHIP CONTRIBUTIONS

SSK formulated the initial concept. RS and SSK designed experiments. RLS, CMR, NY, MJC, ELS, MH, and CLF performed CART experiments; SS performed western blot experiments; MJC, RLS, and CMS performed and analyzed the RNA-sequencing experiment; RLS analyzed the data and prepared the figures; NEK and SSK supervised the study. RLS and SSK wrote the manuscript. All authors edited and approved the final version of the manuscript.

effector functions. AXL inhibition is a novel strategy to enhance CART-cell functions through two independent, but complementary, mechanisms: targeting Th2 cells and reversing myeloid-induced CART-cell inhibition through selective targeting of M2-polarized macrophages.

Keywords

chimeric antigen receptor T cells; CART-cell therapy; AXL; AXL inhibition; TP-0903; macrophages

INTRODUCTION

AXL is a member of the Tyro3, AXL, and proto-oncogene tyrosine-protein kinase Mer (TAM) family of receptor tyrosine kinases (RTKs), which are comprised of two immunoglobulin-like and two fibronectin type III repeats in their extracellular domain, a transmembrane domain, and a cytoplasmic protein tyrosine kinase (1). Growth arrest-specific protein 6 (Gas6) is the ligand for the TAM family and binds the receptors with different affinities: AXL > Tyro3 > Mer (1,2). AXL is expressed in a variety of cancers and has been shown to play important multiple roles in regulating tumor cell survival (1–5). The Gas6/AXL axis has been reported to be involved in epithelial to mesenchymal transition, drug resistance, cancer cell survival, tumor progression, and metastasis (6,7). We and others have reported that AXL inhibition results in strong anti-tumor activity in human malignancies through the significant downregulation of anti-apoptotic proteins (8). Several clinical trials investigating the role of AXL inhibition in human malignancies are currently ongoing (NCT03965494, NCT03990454, NCT04004442, NCT02922777, NCT03654833, NCT04681131, NCT03425279, NCT02219711, and NCT02729298).

In addition to its direct anti-apoptosis effect on cancer cells, targeting AXL in animal tumor models has been shown to overcome drug resistance through the subsequent induction of immune cell infiltration into tumors, suggesting a role for AXL in potentiating immune responses (2). To this end, it has been shown that AXL is expressed on multiple types of immune cells, including dendritic cells (DCs), macrophages, and regulatory T cells (Tregs) (3–5). In asthmatic lung mouse models, blockade of AXL enhances innate antiviral immune responses in the lung via effects on type 1 interferon (IFN) generation and inhibition of Th2-driven allergic inflammatory responses (9). AXL expression on immune cells is an independent mechanism of resistance to immune checkpoint blockade in animal models (10), and AXL has also been implicated in resistance to checkpoint blockade in patients with melanoma (11). A recent analysis indicates that tumors from non-responders to checkpoint blockade express high levels of AXL (12). The combination of AXL blockade with immune checkpoint blockade leads to synergistic anti-tumor activity in preclinical tumor models (7). Collectively, these findings indicate involvement of the AXL pathway in resistance to immunotherapy. In this context, we sought to investigate the role of AXL inhibition in overcoming resistance to adoptive T-cell therapy.

Chimeric antigen receptor T (CART)-cell therapy has evolved as a potent and potentially curative therapy in a subset of patients with hematological malignancies (13–19). However, even in initially responsive patients, most relapse or develop resistance within the first year

of treatment (20,21). Additionally, the efficacy of CART-cell therapy in solid tumors is extremely limited, and objective responses are rarely observed (22). Mechanisms of CART-cell failure include intrinsic T-cell defects, T-cell inhibition in the tumor microenvironment, or other tumor escape mechanisms (23–25). To this end, we hypothesized that AXL expression on immune cells limited CART-cell activity, and we aimed to determine the impact of AXL inhibition on CART-cell phenotype and function. We utilized two strategies to inhibit AXL – small molecule AXL inhibitors and genetic disruption of *AXL* in CART cells – and studied the effects on CART-cell phenotype and function.

MATERIALS AND METHODS

Cell lines

JeKo-1 and Molm-13 cells were originally obtained from American Tissue Culture Collection (ATCC). For the indicated experiments, JeKo-1 and Molm-13 cells were transduced with a firefly luciferase ZsGreen (Addgene) and then sorted based on ZsGreen^{+} cells with BD FACSAria IIu SORP cell sorter (BD Biosciences) to obtain a >99% positive population as previously described (26,27). Cell lines were cultured in R10 medium made with Roswell Park Memorial Institute (RPMI) 1640 (Gibco), 10% fetal bovine serum (FBS, MilliporeSigma), and 1% penicillin-streptomycin-glutamine (PSG, Gibco). We confirmed that JeKo-1 cells robustly expressed *AXLAXL* on their surface (Supplementary Fig. S1). 293T cells were obtained from ATCC for lentiviral production. Cells were maintained in D10 medium composed of Dulbecco's modified eagle medium (DMEM, Corning), 10% FBS, and 1% PSG. When indicated, cells were lethally irradiated at 120Gy using a ^{137}Cs irradiator (JL Shepherd & Associates). All cell lines were tested and confirmed negative for mycoplasma (IDEXX).

Primary patient or healthy donor samples

Peripheral blood mononuclear cell (PBMC) isolation: Peripheral blood samples from de-identified normal donor blood apheresis cones (n=24) (28) were obtained under a Mayo Clinic Institutional Review Board (IRB)-approved protocol, and PBMCs were isolated using SepMate™-50 tubes (STEMCELL Technologies). For the density gradient medium, Lymphoprep™ containing alpha-D-glucopyranoside, beta-D-fructofuranosyl homopolymer, and, 3-(acetylamino)-5-(acetylmethylamino)-2,4,6-triodobenzoic acid monosodium salt was used.

T-cell isolation: T cells were separated with RoboSep™-S (STEMCELL Technologies) using negative selection magnetic beads in the EasySep™ Human T-cell Isolation Kit (STEMCELL Technologies). During PBMC or T-cell isolation, RoboSep™ Buffer containing PBS (Gibco), 0.2 g/L potassium chloride, 0.2 g/L potassium phosphate monobasic, 8 g/L sodium chloride, 1.15 g/L sodium phosphate dibasic, and 2% FBS (STEMCELL Technologies) was used.

Leukemic B-cell isolation: Peripheral blood specimens were obtained from solid tumor patients (n=3) enrolled in a TP-0903-based clinical trial (NCT02729298) by Tolero Pharmaceuticals, Inc. and sent to the Mayo Clinic according to a research agreement

between Tolero and the Mayo Clinic. CLL peripheral blood specimens were obtained from the prospectively maintained Mayo Clinic CLL biobank under an IRB-approved protocol (IRB 1827–00). Leukemic B cells were separated with EasySep™ Human B-cell Enrichment Kit (STEMCELL Technologies). Similar to the T-cell isolation described above, B-cell isolation was performed using RoboSep™. The purity of leukemic B cells was confirmed with flow cytometry (>95% $CD19^+$ cells).

Treg isolation: $CD4^+$ T cells derived from healthy donors were enriched by negative selection and subsequently segregated into a $CD4^+CD25^+CD127^{low}$ subpopulation by magnetic bead separation using EasySep Human Regulatory T-cell Isolation Kit (STEMCELL Technologies). Following this, $CD4^+CD25^+CD127^{low}$ cells were sorted on a FACSAria III sorter (BD Biosciences Pharmingen) to obtain $CD4^+CD25^{high}$ $CD127^{low}CD45RA^+$ Tregs (purity of >90%).

Generation of CAR constructs and CART cells

The use of recombinant DNA in the laboratory was approved by the Mayo Clinic Institutional Biosafety Committee (IBC), IBC #HIP00000252.20. The murine anti-human CD19 CAR (CAR19) plasmid was generated by cloning anti-CD19 scFv (accession 7URV_D) (26,27,29,30), CD8 hinge and transmembrane domain, 4–1BB costimulatory domain (accession AAA53133), and CD3ζ signaling domain into a lentiviral backbone (Supplementary Fig. S2A) as previously described (24,26,27,31,32). CART cells were generated according to the published protocols without modifications. T cells from normal healthy donors (n=18) were expanded *in vitro* with anti-CD3/CD28 Dynabeads (Invitrogen, Life Technologiesadded on day 0 of culture) at a bead:cell ratio of 3:1. T cells were transduced with lentiviral supernatant from 293T cells transfected with pLV-CAR19 plasmid and two helper plasmids on day 1 at a multiplicity of infection (MOI) = 3 (Supplementary Fig. S2B). The anti-CD3/CD28 Dynabeads were removed on day 6, and flow cytometric analysis for CAR expression was performed with goat anti-mouse IgG (H+L) cross-adsorbed secondary antibody (Alexa Fluor 647; Invitrogen, Life Technologies) (Supplementary Fig. S2C). Untransduced T cells (UTD) or CART19 cells were grown in T-cell media (TCM) [X-VIVO™ 15 media (Lonza), 10% human AB serum (Corning), 1% penicillin-streptomycin-glutamine (Gibco)] for up to 8 days and then cryopreserved for future experiments. Prior to all experiments, T cells were thawed and rested overnight at 37°C, 5% CO_2 (26,27).

Generation of AXL^{KO} CART19 cells

We selected a guide (g)RNA targeting the second exon of human *AXL* (5'-AACCTGGAGCTGACACCGAA-3'), which was reported previously (33). The gRNA was then cloned into the pLenti CRISPRv2 (GenScript), a lentiviral vector carrying Cas9 and gRNA under the control of a U6 promoter (34). AXL^{KO} CART19 cells were then manufactured via dual transduction of CAR19 and CRISPR lentiviruses as indicated above. The disruption efficiency of CRISPR/Cas9 *AXL* knockout was determined using targeted sequencing through PCR (polymerase chain reaction) and TIDE (Tracking of Indels by Decomposition) analysis, with the latter using the available software at https://tide.nki.nl/ as previously described (31,35). In brief, DNA was isolated from $2–3\times10^6$

AXL^{WT} (wild-type) or AXL^{KO} CART cells using the DNeasy Blood & Tissue Kit (Qiagen), and genomic DNA was PCR-amplified using the GoTaq® Green Master Mix (Promega) with the following primers: TCTGTGACTGTATCCCCCCT (Forward) and CATGCTCAAAGCCGCACG (Reverse). A T100 Thermal Cycler (Biorad) was used. Then, the PCR product was purified prior to sequencing using a Wizard® SV Gel and PCR Clean-Up System (Promega). Lastly, samples were sent to GENEWIZ for Sanger sequencing (ABI 3730xl DNA analyzer). Once the sequences were sent to our lab, we aligned them, along with our selected gRNA using the TIDE bioinformatics tool in order to assess the percentage of gene editing efficiency. AXL^{WT} CART19 (control) cells were generated using a non-targeting scrambled gRNA, which was established as follows: LentiCRISPRv2 vector (Addgene) was first digested with *BsmB*I, and the non-targeting control gRNA sequence, GCACTTTGTTTGGCCTACTG, was ligated into the LentiCRISPRv2 vector at the *BsmB*I site (34).

TP-0903

TP-0903 was obtained from Tolero Pharmaceuticals, Inc.. For *in vitro* experiments (as indicated below), TP-0903 was dissolved in dimethyl sulfoxide (DMSO, Millipore Sigma) and diluted to 10, 30, or 65 nM in TCM. For *in vivo* experiments, TP-0903 powder was dissolved in 5% (w/v) vitamin E TPGS (Millipore Sigma) + 1% (v/v) Tween80 (Millipore Sigma) in deionized water and used as indicated.

Monocyte/macrophage differentiation

Fresh blood samples from healthy donors were collected, and PBMCs were isolated by density gradient centrifugation using SepMate-50 tubes (STEMCELL Technologies). Isolation of monocytes was performed using the classical monocyte isolation kit (Miltenyi Biotec) according to the manufacture's protocol. After isolation of $CD14^+$ monocytes, cells were cultured in ImmunoCult™-SF Macrophage Medium (STEMCELL Technologies) along with 5 μg/mL recombinant human recombinant macrophage colony stimulating factor (M-CSF, STEMCELL Technologies). Monocytes were then cultured at 37°C in a humidified incubator with 5% CO_2 until day 4. For M1 differentiation, 10 ng/mL LPS (MilliporeSigma) and 50 ng/mL IFNγ (STEMCELL Technologies) were added to the culture. For M2 differentiation, 10 ng/mL IL4 (STEMCELL Technologies) was added to the culture according to the manufacture's protocol. Macrophages were harvested on day 6 and used in the following assays as indicated.

Treg suppression assay

Effector T cells (Teff were isolated from healthy donors with similar techniques as described above using SepMate™ tubes and the EasySep™ Human T-cell Isolation Kit. Teff were stained with carboxyfluorescein succinimidyl ester (CFSE; Invitrogen). Tregs and CFSE-stained Teff were then co-cultured at the indicated Treg:Teff ratios in the presence or absence of 30 nM TP-0903 for 4 days. At the end of the culture, cells were stained as indicated below, and flow cytometric analysis was performed. Percent suppression of Teff was calculated based on the percent dividing cells.

Multi-parametric flow cytometry

Anti-human antibodies were purchased from Biolegend (San Diego), eBioscience (San Diego), or BD Biosciences (San Diego), and they are listed in Supplementary Table S1. The preparation of samples for flow cytometry was described previously (26,27). For cell number quantitation, CountBright beads (Invitrogen) were used according to the manufacturer's instructions. In all analyses, the population of interest was gated based on forward vs. side scatter characteristics, followed by singlet gating, followed by live cells gating (LIVE/DEAD™ Fixable Aqua Dead Cell Stain Kit; Invitrogen). One hundred thousand live cells were collected in each assay. Flow cytometry was performed on a three-laser CytoFLEX (Beckman Coulter). All analyses were performed using FlowJo X10.0.7r2 software.

In vitro T-cell function assays

Proliferation assays: Prior to the start of the coculture, healthy donor naïve T cells or CART19 cells were labeled with CFSE. Cells were then re-suspended in TCM at 2×10^6/mL, and cells (50 μL per well) were seeded in 96-well plates. TP-0903 was added to the corresponding wells with final concentrations of 10, 30, or 65 nM. Each assay also included cells with media only as a blank control, cells with 5 ng/mL phorbol 12-myristate 13-acetate (PMA) (Milllipore Sigma) and 0.1 μg/mL ionomycin (Milllipore Sigma) as a positive control, and cells with DMSO as a negative control. After 120 hours, cells were harvested and stained with APC-H7 anti-human CD3 (eBioscience), BV421 anti-human CD4 (BioLegend) (Supplementary Table S1), and LIVE/DEAD™ Fixable Aqua. Cells were then assessed via flow cytometry using the protocol described above. CountBright beads were added prior to flow cytometric analysis to determine the absolute counts.

Cytotoxicity assays: Cytotoxicity assays were performed as previously described (26,27). In brief, luciferase$^+$ JeKo-1 (CD19$^+$) or luciferase$^+$ Molm-13 (CD19$^-$) cells were used as target cells. CART19 cells were co-cultured with target cells at the indicated effector: target (E:T) ratios in TCM. Different concentrations of TP-0903 (10, 30, 65 nmol/mL) or DMSO were added into cultures. Each assay also included control untransduced T cells (UTD, generated from the same donor and expanded under the same conditions), and a negative control target cell line only. Killing was calculated by bioluminescence imaging on a Xenogen IVIS-200 Spectrum (PerkinElmer) at 24, 48, and 72 hours, as indicated in the specific experiment. The CART-cell cytotoxicity assay against malignant B cells from CLL patients was performed as follows: CART19 were co-cultured at different E:T ratios with leukemic B cells. After 48 hours, cytotoxicity was determined by flow cytometry. Live B cells were identified as CD20$^+$ CD3$^-$ and LIVE/DEAD$^-$ cells.

Degranulation and intracellular cytokine assays: Degranulation of both naïve T cells and CART19 cells was performed as previously described (26,27). Briefly, CART19 cells weretreated with TP-0903 incubated with CD19$^+$ JeKo-1 cells at an effector: target ratio of 1:5. When naïve T cells were used as effector cells, PMA (50 ng/mL) and ionomycin (1 μg/mL) was used as stimulators. FITC anti-human CD107a (BD Pharmingen), anti-human CD28 (BD Biosciences), anti-human CD49d (BD Biosciences, San Diego, CA, USA) (Supplementary Table S1) and monensin (Biolegend) were added prior to the

incubation. After 4 hours, cells were harvested and stained with LIVE/DEAD™ Fixable Aqua. Cells were then fixed and permeabilized (FIX & PERM Cell Fixation & Cell Permeabilization Kit, Life Technologies) and stained with APC anti-human CD3 (clone UCHT1; eBioscience) or BV605 anti-human CD3 (clone SK3; Biolegend) and intracellular cytokines: PE-CF594 anti-human IL2 (clone 5344.111; BD Pharmingen), BV421 anti-human GM-CSF (clone BVD2–21C11; BD Pharmingen), APC-eFluor 780 anti-human IFNγ (clone 4S.B3; Invitrogen), PE-Cy7 anti-human IL13 (clone JES10–5A2; Biolgend), APC anti-human IL4 (clone MP4–25D2; BD Pharmingen), and Alexa fluor 700 anti-human TNFα (clone D21–1351; BD Pharmingen). Cells were then assessed via flow cytometry using the protocol described above.

AXL surface staining: To determine AXL expression on T cells, JeKo-1, isolated monocytes, and differentiated macrophages, cells were stained with goat anti-human AXL affinity-purified polyclonal antibody (Catalog # AF154, R&D Systems), followed by APC-conjugated anti-goat IgG secondary antibody (Catalog # F0108, R&D Systems) and assessed via flow cytometry as described.

Cytokine analysis

Cytokine analysis was performed on cell supernatant obtained from the proliferation assays at 72 hours. Debris was removed from the supernatant by centrifugation at 10,000 x *g* for 5 minutes. Supernatants were then diluted 1:2 with assay buffer (provided with the kit by the manufacturer), before following the manufacturer's protocol for Milliplex Human Cytokine/Chemokine MAGNETIC BEAD Premixed 38 Plex Kit (HCYTMAG-60K-PX38, Millipore Sigma). Data were collected using Luminex (Millipore Sigma).

Western blot analysis

CART cells treated with different doses of AXL inhibition or vehicle control were centrifuged at 100,000 x *g* for 3 hours at 4°C, washed with PBS, and centrifuged again following the same conditions. Pellets were resuspended in 100 μL of radioimmunoprecipitation assay (RIPA) buffer (Boston Bioproducts), and protein concentration was measured by bicinchoninic acid (BCA) protein assay (Pierce Thermo Scientific). 30 μg of protein lysates were used for SDS-PAGE electrophoresis. Following transfer, nitrocellulose membranes (BioRad) were blocked with 5% bovine serum albumin (Millipore Sigma) in tris buffered saline with tween (TBST) (BioRad) for 1 hour at room temperature. Membranes were incubated overnight at 4°C with the following antibodies: rabbit pSAPK/JNK (Thr183/Tyr185; Cell Signaling Technology; dilution 1:1000), rabbit JNK (Cell Signaling Technology, Danvers, MA, USA; dilution 1:1000), rabbit pMAPK (Thr180/Tyr182; Cell Signaling Technology; dilution 1:1000), rabbit MAPK (Cell Signaling Technology; dilution 1:1000), rabbit pLCK (Y34; Abcam; dilution 1:1000), LCK (Abcam; dilution 1:1000), rabbit GATA-3 (BD Biosciences; dilution 1:1000), and rabbit T-bet (eBioscience; dilution 1:1000). Membranes were then washed with TBST and incubated with horseradish peroxidase (HRP)-conjugated secondary antibodies (Cell Signaling) at a dilution of 1:10,000 for 1 hour at room temperature, followed by visualization using the SuperSignal West Pico Plus Chemiluminescence substrate (Thermo Fisher).

In vivo mouse experiments

6–8-week-old non-obese diabetic/severe combined immunodeficient mice bearing a targeted mutation in the interleukin (IL)-2 receptor gamma chain gene (NSG) mice were originally obtained from Jackson Laboratories (Jackson Laboratories) and then maintained at the Mayo Clinic animal facility. All animal experiments were performed under an IACUC approved protocol (IACUC A00001767). Mice were maintained in an animal barrier space that was approved by the IBC for BSL2+ level experiments (IBC #HIP00000252.20). Mice were observed twice a week. At the sign of any clinical instability or deterioration, they were observed daily. Body condition scores (1–5) were recorded and monitored over time (36). Mice that developed a body condition score of 1 or 2 were euthanized. When mice developed any signs of hind-limb paralysis, inability to ambulate or access food/water, we defined these as humane endpoints, and mice were euthanized with carbon dioxide overdose followed by cervical dislocation. Mice were intravenously injected with 1.0×10^6 luciferase$^+$ JeKo-1 cells. 7 or 14 days after injection, mice were imaged with a bioluminescent imager using a Xenogen IVIS-200 Spectrum camera (PerkinElmer) to confirm engraftment. Imaging was performed 10 minutes after the intraperitoneal injection of 10 μL/g D-luciferin (15 mg/mL, Gold Biotechnology). Mice were then randomized based on their bioluminescence imaging to receive different treatments as outlined in the separate specific experiments. Mice were euthanized for necropsy on day 49 To assess CART-cell expansion *in vivo*, mice were bled 17 days after CART19-cell administration. Hundred micro litter of blood was harvested from tail vein bleeding into Microvette capillary blood tubes (Sarstedt INC MS). 70 μL of blood was lysed with RBC lysing solution (BD Biosciences). Cells were then stained with APC-eFluor780 anti-mouse CD45 (clone 30-F11; Invitrogen, Life Technologies), BV421 anti-human CD45 (clone HI30; Biolegend), PE-Cy7 anti-human CD3 (clone OKT3; Biolegend), and APC anti-human CD20 (clone 2H7; Biolegend) (Supplementary Table S1). Circulating T cells were assessed via flow cytometry as indicated above and were gated via mouse CD45$^-$ human CD45$^+$CD3$^+$CD20$^-$ population. Absolute number of T cells was calculated using the volume metrics (37,38). After euthanasia, spleens, femurs, and tibias were harvested. Harvested spleens were processed into single-cell suspensions as previously described (39). To obtain bone marrow cells, RPMI was used to flush out bone marrow from the femurs and tibias (32).

RNA-sequencing (RNA-seq) and analysis

CART19 cells from three biological replicates were thawed and stimulated with intact JeKo-1 cells at a one-to-one ratio for 24 hours. Each sample was treated with either 30 nM TP–0903 (treated condition) or 3.9 μL/mL DMSO (untreated control). CART19 cells were isolated by using CD4 and CD8 microbeads (Miltenyi, positive selection), and isolation was performed twice to eliminate possible contamination by JeKo-1 cells . During the magnetic cell separation, QuadroMACS™ Separator (Miltenyi) and LS Columns (Miltenyi) were used. RNA was isolated from the CART19 cells using the QIAGEN RNeasy Plus Mini Kit (QIAGEN). RNA was further treated with DNase I (QIAGEN) and purified using RNA Clean & Concentrator (Zymo Research). RNA-seq was performed on an Illumina HTSeq 2000 by the Genome Analysis Core at Mayo Clinic. In brief, RNA libraries were prepared using 200 ng total RNA according to the manufacturer's instructions for the TruSeq Stranded mRNA Sample Prep Kit (Illumina). The concentration and size distribution of the

completed libraries were determined using an Agilent Bioanalyzer DNA 1000 chip (Agilent Technologies) and Qubit fluorometry (Invitrogen). Libraries were sequenced at 9 samples per flow cell following Illumina's standard protocol for the NextSeq 2000. The NextSeq P2 flow cell was sequenced as 100 × 2 paired-end reads using NextSeq 1000/2000 Control Software Suite v1.4.1 and RTA3. Raw fastq data files were obtained from the Bioinformatics Core. Fastq files were viewed in FastQC to check for quality (37). After verifying the lack of adapter sequences with FastQC (40), Cutadapt (41) was used to filter for reads greater than 32 base pairs. Output files were re-checked for quality using FastQC. The latest human reference genome (GRCh38.p13) was downloaded from NCBI. Genome index files were generated using STAR (37,42). Paired end reads from fastq files were mapped to the genome for each condition. HTSeq was used to generate expression counts for each gene (37,43). DeSeq2 was used to calculate differential expression using p-values ($\alpha = 0.05$) (37,44). The pheatmap package was used to generate a heatmap and the EnhancedVolcano package was used to create a volcano plot for significantly differentially expressed genes (p-value < 0.05). QIAGEN Ingenuity pathway analysis (IPA) software was used to explore the top canonical pathways and top upstream regulators associated with the significantly differentially expressed genes (p-value < 0.05) (45). In order to determine disruption efficiency of CRISPR/Cas9 GM-CSF knockout using targeted sequencing through PCR (Polymerase Chain Reaction) and TIDE (Tracking of Indels by Decomposition) analysis, the latter using the available software at https://tide.nki.nl/ as previously described (31).

Statistical analysis

Prism Graph Pad and Microsoft Excel (Microsoft) were used to analyze the experimental data. Statistical tests are described in the figure legends. Briefly, normally distributed data were tested by one- and two-way analysis of variance (ANOVA), followed by Dunnett's multiple comparisons test, and unpaired and paired two-sample Student's t-test or Mann–Whitney U test were used for two-group comparisons. Survival was estimated using the Kaplan-Meier curve and Log-rank test was used to test the hypotheses for *in vivo* survival.

Data and materials availability

The data generated in this study are publicly available in Gene Expression Omnibus (GEO) at GSE199257.

RESULTS

AXL is expressed on CART cells and differentiated myeloid cells

First, we aimed to assess the expression of AXL on T-cell subsets, CART cells, and activated CART cells. Our results indicated that both T cells and CART cells expressed AXL, which was further induced upon activation (Figure 1A, Supplementary Fig. S3A). CD19-directed CART (CART19) cells that were activated, either non-specifically [via phorbol 12-myristate-13-acetate (PMA) and ionomycin] or via their CAR (by a co-culture with lethally irradiated $CD19^+$ mantle cell lymphoma (MCL) cell line JeKo-1), expressed significantly higher levels of AXL, compared to resting CART19 cells, as determined by flow cytometry (Fig. 1A). There was significantly higher AXL expression on Th2 CART19 cells compared to Th1 CART19 after their stimulation (Fig. 1B, Supplementary Fig. S3B-

C). Western blotting confirmed our flow cytometric findings and demonstrated significant expression of AXL on both UTD and CART19 cells (Fig. 1C). Analysis of innate immune cells also revealed significant AXL expression on monocytes (Fig. 1D, Supplementary Fig. S3D), similar to prior reports (46). In addition, M2-polarized macrophages expressed higher levels of AXL compared to M1-polarized macrophages (Fig. 1E, Supplementary Fig. S3E-F) (9,47,48).

AXL inhibition selectively reduces inhibitory Th2 cytokines

Having shown that AXL expression was induced on activated T cells, we aimed to determine the effects of AXL inhibition on T-cell functions. When T cells isolated from peripheral blood mononuclear cells (PBMCs) of normal donors were stimulated with PMA (50 ng/mL) and ionomycin (1 μg/mL) in the presence of the highly specific AXL inhibitor TP-0903 (see methods regarding the selection of this AXL inhibitor), there was a significant reduction of the immunosuppressive cytokines, IL4 and IL13, while production of Th1 cytokines and effector cytokines (IL2 and IFNγ) were preserved (Fig. 2A). This suggested to us a selective targeting of Th2 cells. To further confirm this, we determined T-cell phenotype by flow cytometry. Here, freshly isolated T cells were stimulated with PMA and ionomycin for 3 days and stained for chemokine receptors. There was a relative increase of the $CCR6^{-}CXCR3^{+}CCR4^{+}$ fraction following AXL inhibition (Fig. 2B).

AXL inhibition of CART cells reduces inhibitory cytokines and enhances CART-cell proliferation

Because our experiments indicated that AXL inhibition modulated activated T-cell phenotype and cytokine production, we aimed to determine whether this effect also applied to CART19 cells. We first evaluated the direct anti-tumor effect of AXL inhibition against malignant B-cell targets, using the $CD19^{+}$ JeKo-1 cells or leukemic B cells derived from chronic lymphocytic leukemia (CLL) patients by performing *in vitro* killing assays. Whereas 65 nM of the AXL inhibitor TP-0903 resulted in direct anti-tumor activity, there was no observed killing of tumor cells at lower doses of the AXL inhibitor TP-0903 (10–30 nM) (Supplementary Fig. S4A and S4C). Of note that we have previously shown that TP-0903 results in potent inhibition of AXL phosphorylation in B-cell malignancies at these lower dose levels (8). To determine the specific effects of AXL inhibition on CART19 cells, independent of its anti-tumor effect, we used the lower doses of TP-0903 (10–30 nM) for the rest of the experiments in this report.

First, we studied the impact of AXL inhibition on CART19 effector functions. CART19 cells were stimulated through the CAR with $CD19^{+}$ JeKo-1 cells at a 1:5 ratio and maintained in culture for 5 days. Treatment with 10 nM of the AXL inhibitor TP-0903 resulted in superior $CD8^{+}$ CART-cell proliferation (Fig. 2C). Immunophenotype of stimulated CART cells by flow cytometry suggested a relative increase in Th1 phenotype following AXL inhibition (Th1 CART cells: $CD4^{+}CCR6^{-}CXCR3^{+}CCR4^{-}$ and $CD4^{+}CCR6^{-}CXCR3^{+}CCR4^{+}$ cells; Th2 CART cells: $CD4^{+}CCR6^{-}CXCR3^{-}CCR4^{+}$ cells; Fig. 2D, lower panel). The effect of AXL inhibition with TP-0903 on Th2 cells was further confirmed by measuring secreted cytokines 24 hours after CART-cell stimulation (via co-culture with irradiated JeKo-1 cells) in the presence of the AXL inhibitor TP-0903.

AXL inhibition of CART cells resulted in a reduction of IL4, IL10, IL6, soluble (s)CD40L, MIP-1β, IP-10, and IL8, but not IFNγ, IL2, TNFα, and IL7 (Fig. 2E).

The lack of anti-tumor activity with low doses of the AXL inhibitor TP-0903 (10–30 nM) (Supplementary Fig. S4A-B) suggested that these observations were related to direct effects on T cells, rather than a direct anti-tumor effect. These results were consistent when experiments were repeated using a different $CD19^+$ cell line or patient-derived $CD19^+$ CLL cells in a co-culture with CART19 cells (Supplementary Fig. S4C-D). Given the well-known difficulty in maintaining primary, patient-derived malignant $CD19^+$ B cells in culture and the consistency of observed trends across $CD19^+$ target cell types, we used the $CD19^+$ JeKo-1 MCL cell line for the rest of the experiments in this report.

TP-0903 is reported to have off-target effects beyond its inhibition of AXL-RTK (49,50). To confirm that CART-cell modulation induced by TP-0903 was due to AXL inhibition, we knocked out the *AXL* gene in CART cells during their manufacturing using the CRISPR/Cas9 system with a guide (g)RNA (33) cloned into a CRISPR lentivirus backbone (27), as shown in Supplementary Fig. S5A-B. AXL was successfully knocked out of CART19 cells (Supplementary Fig. S6A-B) with a knockout efficiency of 73.2% (n=3, 67.9–83.2%, Supplementary Figure S7). Control CART19 cells were generated using a CRISPR/Cas9 scramble control guide RNA (AXL^{WT} CART19), as previously reported by our laboratory (31). We then evaluated T-cell phenotype and function of AXL^{WT} CART19 or AXL-knockout CART19 (AXL^{KO} CART19) cells after co-culture with JeKo-1 cells for 3 days via flow cytometry. Similar to AXL inhibition with TP-0903, AXL^{KO} CART19 cells showed significant reduction of Th2 cells and increased Th1 subsets (Supplementary Fig. S8A). Disruption of AXL in CART19 cells did not impair their immediate functions *in vitro* (Supplementary Fig. S8B-C).

AXL inhibition with TP-0903 improves anti-lymphoma activity and CART-cell expansion *in vivo*

To further validate the impact of AXL inhibition with TP-0903 on CART cells *in vivo*, we used a JeKo-1-xenograft NOD-SCID-$\gamma^{-/-}$ (NSG) mouse model. We first tested TP-0903 and CART19 combination therapy in a JeKo-1 relapse mouse model with higher tumor burden. Here, luciferase$^+$ JeKo-1 cells (1.0×10^6) were intravenously injected into NSG mice. Engraftment was confirmed 14 days after the implantation, and tumor burden was assessed with bioluminescent imaging (BLI). Mice were then randomized based on their BLI to receive control vehicle, a low dose of AXL inhibitor TP-0903 monotherapy, CART19 monotherapy, or combination TP-0903 and CART19 cells. TP-0903 and CART19 combination therapy resulted in superior anti-tumor activity (Fig. 3A-B) and significantly longer overall survival compared to CART19 monotherapy [Fig. 3C, hazard ratio (HR) = 0.089 with 95% confidence interval (CI) (0.01595 to 0.5072), p=0.004]. Peripheral blood was collected 17 days after CART19 administration and circulating CART19 cells were measured. The combination of TP-0903 and CART19 cells resulted in enhanced CART19 expansion compared to CART19 monotherapy (CART19 + vehicle) (Fig. 3D). In order to assess CART19cell phenotype, a subset of mice were euthanized at day 17 of CART19 cell treatment, and spleens were harvested. Flow cytometric analysis of splenocytes revealed

significant Th1 polarization of CART19 cells in mice treated with TP-0903 in combination with CART19 cells (Fig. 3E). AXL inhibitor TP-0903 monotherapy did not have any significant anti-tumor activity at the low doses used in this model. This further validated that the significantly enhanced anti-tumor activity of CART19 cells in this model is a result of direct modulation of CART19 cells by TP-0903.

AXL inhibition with TP-0903 results in T cell–phenotype changes in patients with solid tumors treated with TP-0903 in a first in human phase I trial

To validate our laboratory findings, we analyzed PBMCs cryopreserved from patients (n=3) with advanced solid tumors treated with TP-0903 in a first in human phase I clinical trial (ClinicalTrials.gov Identifier: NCT02729298). Our results indicated that 24 hours after treatment with TP-0903, there was an alteration in T-cell phenotype, with a relative increase in Th1 T cells ($CD4^+CCR6^-CXCR3^+CCR4^+$), based on immunophenotype analyses by flow cytometry (Fig. 4A), validating our *in vitro* findings (Fig. 2). We also found a significant reduction of Tregs after TP-0903 treatment (Fig. 4B). To study the effect of AXL inhibition on Tregs *ex vivo*, we performed an *in vitro* Treg suppression assay. PBMCs derived from healthy donors were co-cultured with Tregs (Supplementary Fig. S9) obtained from healthy donors at the indicated ratios. Flow cytometric analysis on day 5 of co-culture indicated that AXL inhibition with TP-0903 significantly reduced Treg suppression (Fig. 4C).

Myeloid cells are sensitive to killing by the AXL inhibitor TP-0903

Given the significant upregulation of AXL on $CD14^+$ monocytes and M2-polarized macrophages, we performed experiments to determine if there were any functional effects of AXL inhibition on monocytes. Freshly isolated PBMCs derived from healthy donors were treated with various concentrations of the AXL inhibitor TP-0903 or DMSO vehicle control for 24 hours. Compared to T cells, monocytes were significantly more sensitive to the AXL inhibitor TP-0903 vs. control vehicle at all concentrations tested, as determined by a reduction of survival measured by flow cytometry (Fig. 5A). These results suggest that, in addition to the direct effects of AXL inhibition on Th2 cells and their secreted cytokine profile, TP-0903 inhibition of AXL has profound and direct activity on monocytes.

AXL inhibition with TP-0903 ameliorates monocyte-induced CART19-cell inhibition

Monocytes and myeloid-derived cytokines have been shown to inhibit CART-cell functions *in vitro* and *in vivo* (26,51,52). Based on the observed effect of AXL inhibition on monocytes as described above, we further probed whether AXL inhibition ameliorated monocyte-induced CART-cell inhibition. Normal healthy donor CART19 cells were cultured with $CD19^+$ JeKo-1 cells in the presence of isolated $CD14^+$ monocytes (>95% purity, Supplementary Fig. S10) at a ratio of 1:5:1 (CART: monocytes: tumor cells), as we have previously shown inhibition of CART cells at this ratio (26,27). Co-cultures were performed in the presence of the AXL inhibitor TP-0903 (30 nM) or vehicle control. Cells were harvested on day 5, and absolute numbers of T cells were counted via flow cytometry. As expected and previously shown (53), there was a significant inhibition of CART19 cell proliferation in the presence of monocytes, but this was reversed when the AXL inhibitor TP-0903 was added to the co-culture (Fig. 5B). Cytokine analysis of supernatants harvested 72 hours after the monocyte/TP-0903 co-culture demonstrated

significant reductions of myeloid-related cytokines, including IL6, IL1 receptor α, IL1β, IL17A, and soluble (s)CD40 ligand in the presence of low doses of TP-0903 (Fig. 5C). This suggested to us a direct effect of the AXL inhibitor TP-0903 on monocyte function. In addition, flow cytometric analysis of myeloid cell subsets following co-culture suggested a selective reduction in M2 macrophages (Fig. 5D-E).

TP-0903 inhibition of CART19 cells is specific for AXL

Having shown that 1) AXL expression was upregulated on activated Th2 and M2 cells, 2) AXL inhibition reduced inhibitory cytokines and synergized with effector T cells and CART19 cells, and 3) AXL inhibition ameliorated myeloid cell-induced T-cell inhibition, we sought to further validate whether the observed effects were due to selective killing of Th2 cells and M2 cells, and not due to off-target effects by the AXL inhibitor TP-0903. We first interrogated downstream signaling through AXL and other potential non-AXL targets for TP-0903. There were no changes in phosphorylation of JNK, p38, GATA-3, T-bet, or LCK in CART19 cells following treatment with low doses (10–30 nM) of TP-0903 (Fig. 6A). Of note, higher doses of TP-0903 are known to have off target effects (8). We then evaluated CART19 transcriptome changes following AXL inhibition. We performed RNA-sequencing on activated CART19 cells after co-culture with $CD19^+$ JeKo-1 cells in the presence of the low-dose (30 nM) TP-0903 or vehicle control for 24 hours. Subsequently, $CD4^+$ and $CD8^+$ T cells were isolated via magnetic sorting, flow cytometric analysis confirmed >99% purified T-cell fractions (Supplementary Fig. S11), and RNA-seq on CART19 cells was performed. 322 significantly upregulated and 414 significantly downregulated genes after treatment with 30 nM of TP-0903 were identified (Fig. 6B-C). QIAGEN Ingenuity Pathway Analysis (IPA) identified the ‘macrophage alterative activation signaling pathway’ as the most significantly altered pathway following AXL inhibition with TP-0903 (Fig. 6D, Supplementary Fig. S12). This pathway associates with immune-suppressive signals, including CXCL13 (54,55), IL4, and IRF4 (56). In addition, the ‘IL33 signaling pathway’ was significantly suppressed when CART19 cells were treated with TP-0903, indicating inhibition of Th2-mediated responses (Supplementary Fig. S13) (57–60). Consistent with the findings of interactions between CART19 and myeloid cells (Fig. 5), pathway analysis identified ‘role of IL17F in allergic inflammatory airway diseases’ and ‘pathogen-induced cytokine storm signaling’ pathways as significantly altered following AXL inhibition with TP-0903 (Supplementary Fig. S14-S15). AXL inhibition significantly promoted the ‘regulation of IL2 expression in activated and anergic T lymphocytes’, ‘T-cell receptor signaling’, and ‘G-protein signaling mediated by Tubby’ pathways (Supplementary Fig. S16-S18). The top five upstream regulators identified with QIAGEN IPA of differentially expressed genes were IL4, TNF, CSF2, TGFβ, and SATB1 (Table 1). Sequencing data are listed in Supplementary Table S2.

DISCUSSION

In this study, we identified for the first time that AXL inhibition enhanced T-cell immunotherapy in preclinical studies and models. Specifically, we showed that this likely occurs via the selective modulation of two key inhibitory immune cells in the microenvironment where AXL is overexpressed: Th2 and M2 cells. Our results demonstrate

that AXL inhibition enhances CART-cell immunotherapy *in vitro* and *in vivo* through the selective suppression of inhibitory immune cells. Our unique findings were also corroborated in this study, in part, by our findings of T-cell modulation, including a reduction of Tregs following treatment of patients with solid tumors with the AXL inhibitor TP-0903.

Immunotherapy with CART19 cell therapy has recently emerged as a potentially curative therapy for patients with B-cell malignancies (13–19). However, challenges to this approach remain, including low rates of durable responses and extremely limited CART-cell activity in solid tumors (22). Correlative studies from pivotal clinical trials demonstrate that mechanisms of CART-cell therapy failure can include tumor antigen escape, intrinsic T-cell defects, and CART-cell inhibition by the tumor microenvironment. Additionally, myeloid-related cytokines have been implicated in resistance in patients receiving CART19-cell therapy (8,25,61).

AXL has recently gained attention as a novel target for cancer therapy. Numerous agents against AXL have been established, including kinase inhibitors and antibodies (6). Although AXL is primarily known to be associated with metastasis and therapeutic resistance, recent data indicate that AXL may also play an important anti-inflammatory and immunomodulatory role (62). AXL is expressed on immune cells and can function to modify cellular function (63). AXL, which is known to be expressed on natural killer cells (63,64) and tumor-associated macrophages (65), is an important negative inflammatory mediator that inhibits innate immune cells and has been implicated in immune suppression (66). This suggests that AXL inhibition would be an excellent candidate to test as a positive modifier of CART-cell activity. We hypothesized that AXL inhibition might enhance CART-cell effector function through two independent but complementary mechanisms: 1) selective suppression of Th2 cells and 2) amelioration of myeloid-induced CART-cell inhibition. To do this work we utilized two strategies: AXL inhibition with TP-0903 and *AXL* knockout using CRISPR/Cas9. TP-0903 is a small molecule with potent inhibitory effects on AXL receptor tyrosine kinase (8). Early results from the first-in-human phase I trial of TP-0903 in patients with advanced solid tumors (NCT02729298) have shown that this compound is well-tolerated and has promising anti-tumor effects. We therefore elected to study the effect of AXL inhibition using this specific molecular therapeutic drug as a potentially translatable therapy to enhance T-cell immunotherapy.

To confirm that the observed effects were due to AXL inhibition, we generated AXL^{KO} CART19 cells and studied their profile. We found higher expression of AXL on activated inhibitory Th2 and M2 immune cells and showed that AXL inhibition selectively reduced Th2- and M2-associated cytokines, with a likely resultant impact on immunotherapy. Upregulation of AXL on activated CART19 cells was induced following their antigen-specific and non-specific stimulation. Our findings that AXL expression on activated CART19 did not require co-culture with tumor cells indicates that AXL upregulation might be independent of Gas6 ligand interactions. This is corroborated by the observed altered CART-cell phenotype, with skewing to a Th1 phenotype following *AXL* knockout, which further suggests an intrinsic role for AXL in CART-cell function. The mechanisms of

this upregulation are being currently investigated and will be reported in a subsequent manuscript.

Our finding of reduced Th2 cytokines is significant. Th2 cytokines have extensive immunosuppressive effects in the tumor microenvironment (67). Consistent with the *in vitro* findings, the most significant upstream regulator identified in IPA for differentially expressed genes was IL4. We recently reported that IL4 is a regulator of CART-cell dysfunction, and we showed that neutralizing IL4 enhances the anti-tumor activity of CART cells in preclinical models (68). IL4 polarizes tumor-directed $CD4^+$ T cells to Th2 phenotypes and reduces the number and cytotoxicity of effector $CD8^+$ T cells. IL4 also polarizes macrophages into suppressive tumor-associated macrophages (also referred to as M2-type macrophages). IL4 plays an important role as a growth factor for various types of malignancies, including B-cell lymphomas (70,71, 72). Therefore, modulating IL4 with AXL inhibition presents a compelling strategy to improve CART-cell therapy.

Our *in vivo* JeKo-1 xenograft model showed that combination therapy with TP-0903 and CART19 cells had improved tumor control compared to CART19-cell monotherapy, suggesting an effective and positive modulation of T-cell phenotype. AXL inhibition of CART19 cells also led to a significantly higher expansion of circulating CART19 cells. This is consistent with prior reports showing that double- and triple-mutant genes in the TAM family result in lympho-proliferation and autoimmunity due to hyper-activation of antigen presenting cells (73). Moreover, CART19 cells within the spleens from mice treated with TP-0903 resulted in Th1 polarization, similar to the *in vitro* findings. Paradoxically, an increase of T-cell proliferation raises concerns that AXL inhibition of CART cells may have a higher risk of CART-cell toxicities, such as cytokine release syndrome (26,52,74,75). However, our data also indicated that AXL inhibition selectively targeted monocytes and reduced their production and secretion of cytokines, which have been implicated as the driver cytokines for the development of CART cell-associated toxicities. Furthermore, IPA identified several pathways that regulated immune inflammation, including cytokine-related signaling, when CART19 cells were treated with the AXL inhibitor TP-0903. These suggest that AXL inhibition of CART cells could have multiple benefits by reducing their toxicity through the selective inhibition of myeloid cells, while also enhancing their proliferation. This will be more formally tested is a dose-escalation phase I clinical trial for the combination of CART19 with the AXL inhibitor TP-0903.

Inhibitory myeloid cells have been implicated in the development of toxicities post-CART-cell therapy, as well as in mediating resistance. The myeloid cytokines IL6, IL1, and GM-CSF have been strongly associated with the development of cytokine release syndrome and neurotoxicity, and IL6-directed therapy is the current mainstay of treatment for these CART-cell toxicities (26,52,74). Infiltration of myeloid cells into the cerebrospinal fluid is significantly associated with the development of neurotoxicity after CART-cell therapy (76). The presence of monocytes in *ex vivo* cultures was found to limit CART-cell expansion (53). Tissue infiltration of myeloid cells restricted CART-cell trafficking and functions in clinical trials of CART-cell therapy in hematological and solid malignancies (51). Collectively, this body of evidence suggests that strategies which target inhibitory monocytes, such as

AXL inhibitors, have the potential to improve CART-cell therapy, while reducing CART cell-associated toxicities.

In summary, we demonstrate in this report a novel impact of AXL inhibition on immune modulation of adoptive T-cell therapy. We have shown for the first time that AXL inhibition modulates CART19 functions to enhance their anti-tumor activity against $CD19^+$ cells through the suppression of Th2 cells and M2 macrophages. Based on this current study, a phase I clinical trial testing the combination of TP-0903 and CART19 cells in relapsed/refractory B-cell malignancies is planned.

Supplementary Material

Refer to Web version on PubMed Central for supplementary material.

ACKNOWLEDGEMENTS

This work was supported through the National Cancer Institute (R37CA266344 (SSK), K12CA090628 (SSK), K99CA273304 (RLS)), Mayo Clinic K2R Career Development Program (SSK), the Mayo Clinic Center for Individualized Medicine (SSK), the Predolin Foundation (RLS), the Eagles Foundation (RLS), Gerstner Family Foundation (RLS), and Tolero Pharmaceutical (SSK and NEK). This work was also supported in part by the Henry J. Predolin Foundation (biobank). We would like to thank Michael W. and Georgia Taylor Michelson for their funding contribution that assisted in supporting this project. The authors are grateful to Brooke L. Kimball, Truc Huynh, and Long K. Mai for their technical assistance.

CONFLICT OF INTEREST

SSK is an inventor on patents in the field of CAR immunotherapy that are licensed to Novartis (through an agreement between Mayo Clinic, University of Pennsylvania, and Novartis). RLS, MJC, and SSK are inventors on patents in the field of CAR immunotherapy that are licensed to Humanigen (through Mayo Clinic). SSK and MH are inventors on patents in the field of CAR immunotherapy that are licensed to Mettaforge (through Mayo Clinic). SSK and IC are inventors on patients that are licensed to Sendero (through Mayo Clinic). SSK is an inventor on intellectual property that is licensed to MustangBio (through Mayo Clinic). SSK receives research funding from Kite, Gilead, Juno, Celgene, Novartis, Humanigen, MorphoSys, Tolero, Sunesis, LeahLabs, and Lentigen. SSK has participated in advisory meetings of Juno, Celgene, Kite, Gilead, LeahLabs, CapstanBio, Torque, Luminary, and Humanigen. SSK has participated in data safety monitoring boards of Humanigen. RLS, LM, JF, SLW, NEK, and SSK are inventors on patents related to this work. NEK receives research funding from Acerta Pharma, BMS, Pharmacyclics, MEI Pharma, and Sunesis. NEK has participated in Advisory Board meetings of Cytomx Therapy, Janssen, Juno Therapeutics, Astra Zeneca, and Oncotracker; and on DSMC for Agios and Cytomx Therapeutics. SAP receives research funding from Pharmacyclics, MorphoSys, Janssen, AstraZeneca, TG Therapeutics, Bristol Myers Squibb, AbbVie, and Ascentage Pharma. SAP has participated in Advisory Board meetings of Pharmacyclics, AstraZeneca, Genentech, Gilead, GlaxoSmithKline, Verastem Oncology, and AbbVie (he was not personally compensated for his participation).

REFERENCES

1. van der Meer JHM, van der Poll T, van ‘t Veer C. TAM receptors, Gas6, and protein S: roles in inflammation and hemostasis. Blood 2014;123:2460–9 [PubMed: 24596417]
2. Vouri M, Hafizi S. TAM Receptor Tyrosine Kinases in Cancer Drug Resistance. Cancer Res 2017;77:2775–8 [PubMed: 28526769]
3. Myers KV, Amend SR, Pienta KJ. Targeting Tyro3, AXL and MerTK (TAM receptors): implications for macrophages in the tumor microenvironment. Molecular cancer 2019;18:94 [PubMed: 31088471]
4. Seitz HM, Camenisch TD, Lemke G, Earp HS, Matsushima GK. Macrophages and dendritic cells use different AXL/Mertk/Tyro3 receptors in clearance of apoptotic cells. J Immunol 2007;178:5635–42 [PubMed: 17442946]

5. Zhao GJ, Zheng JY, Bian JL, Chen LW, Dong N, Yu Y, et al. Growth Arrest-Specific 6 Enhances the Suppressive Function of CD4(+)CD25(+) Regulatory T Cells Mainly through AXL Receptor. Mediators Inflamm 2017;2017:6848430
6. Zhu C, Wei Y, Wei X. AXL receptor tyrosine kinase as a promising anti-cancer approach: functions, molecular mechanisms and clinical applications. Molecular cancer 2019;18:153 [PubMed: 31684958]
7. Okura N, Nishioka N, Yamada T, Taniguchi H, Tanimura K, Katayama Y, et al. ONO-7475, a Novel AXL Inhibitor, Suppresses the Adaptive Resistance to Initial EGFR-TKI Treatment in EGFR-Mutated Non-Small Cell Lung Cancer. Clin Cancer Res 2020;26:2244–56 [PubMed: 31953310]
8. Sinha S, Boysen J, Nelson M, Secreto C, Warner SL, Bearss DJ, et al. Targeted AXL Inhibition Primes Chronic Lymphocytic Leukemia B Cells to Apoptosis and Shows Synergistic/Additive Effects in Combination with BTK Inhibitors. Clinical cancer research : an official journal of the American Association for Cancer Research 2015;21:2115–26 [PubMed: 25673699]
9. Shibata T, Habiel DM, Coelho AL, Kunkel SL, Lukacs NW, Hogaboam CM. AXL receptor blockade ameliorates pulmonary pathology resulting from primary viral infection and viral exacerbation of asthma. J Immunol 2014;192:3569–81 [PubMed: 24659691]
10. Guo Z, Li Y, Zhang D, Ma J. AXL inhibition induces the antitumor immune response which can be further potentiated by PD-1 blockade in the mouse cancer models. Oncotarget 2017;8:89761–74
11. Tsukita Y, Fujino N, Miyauchi E, Saito R, Fujishima F, Itakura K, et al. AXL kinase drives immune checkpoint and chemokine signalling pathways in lung adenocarcinomas. Molecular cancer 2019;18:24 [PubMed: 30744655]
12. Sensi M, Catani M, Castellano G, Nicolini G, Alciato F, Tragni G, et al. Human Cutaneous Melanomas Lacking MITF and Melanocyte Differentiation Antigens Express a Functional AXL Receptor Kinase. Journal of Investigative Dermatology 2011;131:2448–57 [PubMed: 21796150]
13. Maude SL, Frey N, Shaw PA, Aplenc R, Barrett DM, Bunin NJ, et al. Chimeric Antigen Receptor T Cells for Sustained Remissions in Leukemia. New Engl J Med 2014;371:1507–17 [PubMed: 25317870]
14. Lee DW, Kochenderfer JN, Stetler-Stevenson M, Cui YK, Delbrook C, Feldman SA, et al. T cells expressing CD19 chimeric antigen receptors for acute lymphoblastic leukaemia in children and young adults: a phase 1 dose-escalation trial. Lancet 2015;385:517–28 [PubMed: 25319501]
15. Gardner R, Finney O, Smithers H, Leger KJ, Annesley CE, Summers C, et al. CD19CAR T Cell Products of Defined CD4:CD8 Composition and Transgene Expression Show Prolonged Persistence and Durable MRD-Negative Remission in Pediatric and Young Adult B-Cell ALL. Blood 2016;128:219
16. Turtle CJ, Hanafi LA, Berger C, Gooley TA, Cherian S, Hudecek M, et al. CD19 CAR-T cells of defined CD4+:CD8+ composition in adult B cell ALL patients. J Clin Invest 2016;126:2123–38 [PubMed: 27111235]
17. Kochenderfer JN, Dudley ME, Feldman SA, Wilson WH, Spaner DE, Maric I, et al. B-cell depletion and remissions of malignancy along with cytokine-associated toxicity in a clinical trial of anti-CD19 chimeric-antigen-receptor-transduced T cells. Blood 2012;119:2709–20 [PubMed: 22160384]
18. Brentjens RJ, Rivière I, Park JH, Davila ML, Wang X, Stefanski J, et al. Safety and persistence of adoptively transferred autologous CD19-targeted T cells in patients with relapsed or chemotherapy refractory B-cell leukemias. Blood 2011;118:4817–28 [PubMed: 21849486]
19. Davila ML, Riviere I, Wang X, Bartido S, Park J, Curran K, et al. Efficacy and Toxicity Management of 19–28z CAR T Cell Therapy in B Cell Acute Lymphoblastic Leukemia. Science Translational Medicine 2014;6:224ra25-ra25
20. Maude SL, Laetsch TW, Buechner J, Rives S, Boyer M, Bittencourt H, et al. Tisagenlecleucel in Children and Young Adults with B-Cell Lymphoblastic Leukemia. N Engl J Med 2018;378:439–48 [PubMed: 29385370]
21. Park JH, Riviere I, Gonen M, Wang X, Senechal B, Curran KJ, et al. Long-Term Follow-up of CD19 CAR Therapy in Acute Lymphoblastic Leukemia. N Engl J Med 2018;378:449–59 [PubMed: 29385376]

22. Wagner J, Wickman E, DeRenzo C, Gottschalk S. CAR T Cell Therapy for Solid Tumors: Bright Future or Dark Reality? Mol Ther 2020;28:2320–39 [PubMed: 32979309]
23. Klebanoff CA, Scott CD, Leonardi AJ, Yamamoto TN, Cruz AC, Ouyang C, et al. Memory T cell-driven differentiation of naive cells impairs adoptive immunotherapy. J Clin Invest 2016;126:318–34 [PubMed: 26657860]
24. Sakemura R, Hefazi M, Siegler EL, Cox MJ, Larson DP, Hansen MJ, et al. Targeting Cancer-Associated Fibroblasts in the Bone Marrow Prevents Resistance to CART-Cell Therapy in Multiple Myeloma. Blood 2022
25. Sakemura R, Cox MJ, Hefazi M, Siegler EL, Kenderian SS. Resistance to CART cell therapy: lessons learned from the treatment of hematological malignancies. Leuk Lymphoma 2021:1–18
26. Sterner RM, Sakemura R, Cox MJ, Yang N, Khadka RH, Forsman CL, et al. GM-CSF inhibition reduces cytokine release syndrome and neuroinflammation but enhances CAR-T cell function in xenografts. Blood 2019;133:697–709 [PubMed: 30463995]
27. Sterner RM, Cox MJ, Sakemura R, Kenderian SS. Using CRISPR/Cas9 to Knock Out GM-CSF in CAR-T Cells. Jove-J Vis Exp 2019
28. Dietz AB, Bulur PA, Emery RL, Winters JL, Epps DE, Zubair AC, et al. A novel source of viable peripheral blood mononuclear cells from leukoreduction system chambers. Transfusion 2006;46:2083–9 [PubMed: 17176319]
29. Siegler EL, Simone BW, Sakemura R, Tapper EE, Horvei P, Cox MJ, et al. Efficient Gene Editing of CART Cells with CRISPR-Cas12a for Enhanced Antitumor Efficacy. Blood 2020;136:6–7 [PubMed: 32614958]
30. Cox MJ, Kuhlmann CJ, Sterner RM, Sakemura R, Sinha S, Mwangi R, et al. Improved Anti-Tumor Response of Chimeric Antigen Receptor T Cell (CART) Therapy after GM-CSF Inhibition Is Mechanistically Supported By a Novel Direct Interaction of GM-CSF with Activated Carts. Blood 2019;134:3868-
31. Cox MJ, Manriquez Roman C, Tapper EE, Siegler EL, Chappell D, Durrant C, et al. GM-CSF disruption in CART cells modulates T cell activation and enhances CART cell anti-tumor activity. Leukemia 2022
32. Sakemura R, Cox MJ, Bansal A, Roman CM, Hefazi M, Vernon CJ, et al. Dynamic Imaging of Chimeric Antigen Receptor T Cells with [18F]Tetrafluoroborate Positron Emission Tomography/Computed Tomography. JoVE 2022:e62334
33. Axelrod HD, Valkenburg KC, Amend SR, Hicks JL, Parsana P, Torga G, et al. AXL Is a Putative Tumor Suppressor and Dormancy Regulator in Prostate Cancer. Mol Cancer Res 2019;17:356–69 [PubMed: 30291220]
34. Sanjana NE, Shalem O, Zhang F. Improved vectors and genome-wide libraries for CRISPR screening. Nat Methods 2014;11:783–4 [PubMed: 25075903]
35. Brinkman EK, Chen T, Amendola M, van Steensel B. Easy quantitative assessment of genome editing by sequence trace decomposition. Nucleic Acids Research 2014;42:e168-e
36. Ullman-Culleré MH, Foltz CJ. Body condition scoring: a rapid and accurate method for assessing health status in mice. Lab Anim Sci 1999;49:319–23 [PubMed: 10403450]
37. Cox MJ, Lucien F, Sakemura R, Boysen JC, Kim Y, Horvei P, et al. Leukemic extracellular vesicles induce chimeric antigen receptor T cell dysfunction in chronic lymphocytic leukemia. Mol Ther 2021;29:1529–40 [PubMed: 33388419]
38. Sakemura R, Bansal A, Siegler EL, Hefazi M, Yang N, Khadka RH, et al. Development of a Clinically Relevant Reporter for Chimeric Antigen Receptor T-cell Expansion, Trafficking, and Toxicity. Cancer Immunol Res 2021;9:1035–46 [PubMed: 34244299]
39. Manriquez Roman C, Sakemura RL, Jin F, Khadka RH, Adada MM, Siegler EL, et al. Assessment of Chimeric Antigen Receptor T Cell-Associated Toxicities Using an Acute Lymphoblastic Leukemia Patient-derived Xenograft Mouse Model. J Vis Exp 2023
40. Andrews S. 2010 FastQC: a quality control tool for high throughput sequence data. <http://www.bioinformatics.babraham.ac.uk/projects/fastqc>.
41. Martin M. Cutadapt removes adapter sequences from high-throughput sequencing reads. 2011 2011;17:3

42. Dobin A, Davis CA, Schlesinger F, Drenkow J, Zaleski C, Jha S, et al. STAR: ultrafast universal RNA-seq aligner. Bioinformatics 2012;29:15–21 [PubMed: 23104886]
43. Putri GH, Anders S, Pyl PT, Pimanda JE, Zanini F. Analysing high-throughput sequencing data in Python with HTSeq 2.0. Bioinformatics 2022
44. Love MI, Huber W, Anders S. Moderated estimation of fold change and dispersion for RNA-seq data with DESeq2. Genome Biology 2014;15:550 [PubMed: 25516281]
45. Krämer A, Green J, Pollard J, Jr., Tugendreich S. Causal analysis approaches in Ingenuity Pathway Analysis. Bioinformatics 2014;30:523–30 [PubMed: 24336805]
46. Fujimori T, Grabiec AM, Kaur M, Bell TJ, Fujino N, Cook PC, et al. The AXL receptor tyrosine kinase is a discriminator of macrophage function in the inflamed lung. Mucosal Immunol 2015;8:1021–30 [PubMed: 25603826]
47. Zahuczky G, Kristóf E, Majai G, Fésüs L. Differentiation and glucocorticoid regulated apopto-phagocytic gene expression patterns in human macrophages. Role of Mertk in enhanced phagocytosis. PLoS One 2011;6:e21349
48. Waterborg CE, Broeren MG, Blaney Davidson EN, Koenders MI, van Lent PL, van den Berg WB, et al. The level of synovial AXL expression determines the outcome of inflammatory arthritis, possibly depending on the upstream role of TGF-β1. Rheumatology 2019;58:536–46 [PubMed: 30508140]
49. Holland SJ, Pan A, Franci C, Hu Y, Chang B, Li W, et al. R428, a Selective Small Molecule Inhibitor of AXL Kinase, Blocks Tumor Spread and Prolongs Survival in Models of Metastatic Breast Cancer. Cancer Res 2010;70:1544–54 [PubMed: 20145120]
50. Myers SH, Brunton VG, Unciti-Broceta A. AXL Inhibitors in Cancer: A Medicinal Chemistry Perspective. Journal of Medicinal Chemistry 2016;59:3593–608 [PubMed: 26555154]
51. Stroncek DF, Ren J, Lee DW, Tran M, Frodigh SE, Sabatino M, et al. Myeloid cells in peripheral blood mononuclear cell concentrates inhibit the expansion of chimeric antigen receptor T cells. Cytotherapy 2016;18:893–901 [PubMed: 27210719]
52. Norelli M, Camisa B, Barbiera G, Falcone L, Purevdorj A, Genua M, et al. Monocyte-derived IL-1 and IL-6 are differentially required for cytokine-release syndrome and neurotoxicity due to CAR T cells. Nat Med 2018;24:739–48 [PubMed: 29808007]
53. Ruella M, Klichinsky M, Kenderian SS, Shestova O, Ziober A, Kraft DO, et al. Overcoming the Immunosuppressive Tumor Microenvironment of Hodgkin Lymphoma Using Chimeric Antigen Receptor T Cells. Cancer Discovery 2017;7:1154–67 [PubMed: 28576927]
54. Tokunaga R, Zhang W, Naseem M, Puccini A, Berger MD, Soni S, et al. CXCL9, CXCL10, CXCL11/CXCR3 axis for immune activation - A target for novel cancer therapy. Cancer Treat Rev 2018;63:40–7 [PubMed: 29207310]
55. Xie Y, Chen Z, Zhong Q, Zheng Z, Chen Y, Shangguan W, et al. M2 macrophages secrete CXCL13 to promote renal cell carcinoma migration, invasion, and EMT. Cancer Cell International 2021;21:677 [PubMed: 34922542]
56. Man K, Gabriel SS, Liao Y, Gloury R, Preston S, Henstridge DC, et al. Transcription Factor IRF4 Promotes CD8(+) T Cell Exhaustion and Limits the Development of Memory-like T Cells during Chronic Infection. Immunity 2017;47:1129–41.e5
57. Pinto SM, Subbannayya Y, Rex DAB, Raju R, Chatterjee O, Advani J, et al. A network map of IL-33 signaling pathway. J Cell Commun Signal 2018;12:615–24 [PubMed: 29705949]
58. Schmitz J, Owyang A, Oldham E, Song Y, Murphy E, McClanahan TK, et al. IL-33, an Interleukin-1-like Cytokine that Signals via the IL-1 Receptor-Related Protein ST2 and Induces T Helper Type 2-Associated Cytokines. Immunity 2005;23:479–90 [PubMed: 16286016]
59. Rak GD, Osborne LC, Siracusa MC, Kim BS, Wang K, Bayat A, et al. IL-33-Dependent Group 2 Innate Lymphoid Cells Promote Cutaneous Wound Healing. J Invest Dermatol 2016;136:487–96 [PubMed: 26802241]
60. Monticelli LA, Osborne LC, Noti M, Tran SV, Zaiss DM, Artis D. IL-33 promotes an innate immune pathway of intestinal tissue protection dependent on amphiregulin-EGFR interactions. Proc Natl Acad Sci U S A 2015;112:10762–7

61. Dubovsky JA, Flynn R, Du J, Harrington BK, Zhong Y, Kaffenberger B, et al. Ibrutinib treatment ameliorates murine chronic graft-versus-host disease. The Journal of clinical investigation 2014;124:4867–76 [PubMed: 25271622]
62. Rothlin CV, Ghosh S, Zuniga EI, Oldstone MB, Lemke G. TAM receptors are pleiotropic inhibitors of the innate immune response. Cell 2007;131:1124–36 [PubMed: 18083102]
63. Lemke G, Rothlin CV. Immunobiology of the TAM receptors. Nat Rev Immunol 2008;8:327–36 [PubMed: 18421305]
64. Paolino M, Choidas A, Wallner S, Pranjic B, Uribesalgo I, Loeser S, et al. The E3 ligase Cbl-b and TAM receptors regulate cancer metastasis via natural killer cells. Nature 2014;507:508–12 [PubMed: 24553136]
65. Ye X, Li Y, Stawicki S, Couto S, Eastham-Anderson J, Kallop D, et al. An anti-AXL monoclonal antibody attenuates xenograft tumor growth and enhances the effect of multiple anticancer therapies. Oncogene 2010;29:5254–64 [PubMed: 20603615]
66. Akalu YT, Rothlin CV, Ghosh S. TAM receptor tyrosine kinases as emerging targets of innate immune checkpoint blockade for cancer therapy. Immunol Rev 2017;276:165–77 [PubMed: 28258690]
67. Pollard JW. Tumour-educated macrophages promote tumour progression and metastasis. Nat Rev Cancer 2004;4:71–8 [PubMed: 14708027]
68. Stewart C, Cox MJ, Sakemura R, Ogbodo EJ, Can I, Roman CM, et al. Abstract 1153: IL-4 depletion leads to the improvement of CART cell therapy. Cancer Res 2023;83:1153-
69. Pangault C, Amé-Thomas P, Ruminy P, Rossille D, Caron G, Baia M, et al. Follicular lymphoma cell niche: identification of a preeminent IL-4-dependent TFH–B cell axis. Leukemia 2010;24:2080–9 [PubMed: 20944673]
70. Carey GB, Semenova E, Qi X, Keegan AD. IL-4 protects the B-cell lymphoma cell line CH31 from anti-IgM-induced growth arrest and apoptosis: contribution of the PI-3 kinase/AKT pathway. Cell Research 2007;17:942–55 [PubMed: 17968425]
71. Janssen EM, Droin NM, Lemmens EE, Pinkoski MJ, Bensinger SJ, Ehst BD, et al. CD4+ T-cell help controls CD8+ T-cell memory via TRAIL-mediated activation-induced cell death. Nature 2005;434:88–93 [PubMed: 15744305]
72. Mantovani A, Sozzani S, Locati M, Allavena P, Sica A. Macrophage polarization: tumor-associated macrophages as a paradigm for polarized M2 mononuclear phagocytes. Trends Immunol 2002;23:549–55 [PubMed: 12401408]
73. Rothlin CV, Lemke G. TAM receptor signaling and autoimmune disease. Curr Opin Immunol 2010;22:740–6 [PubMed: 21030229]
74. Giavridis T, van der Stegen SJC, Eyquem J, Hamieh M, Piersigilli A, Sadelain M. CAR T cell-induced cytokine release syndrome is mediated by macrophages and abated by IL-1 blockade. Nat Med 2018;24:731–8 [PubMed: 29808005]
75. Sakemura R, Terakura S, Watanabe K, Julamanee J, Takagi E, Miyao K, et al. A Tet-On Inducible System for Controlling CD19-Chimeric Antigen Receptor Expression upon Drug Administration. Cancer Immunology Research 2016;4:658–68 [PubMed: 27329987]
76. Santomasso BD, Park JH, Salloum D, Riviere I, Flynn J, Mead E, et al. Clinical and Biological Correlates of Neurotoxicity Associated with CAR T-cell Therapy in Patients with B-cell Acute Lymphoblastic Leukemia. Cancer Discov 2018;8:958–71 [PubMed: 29880584]

SYNOPSIS

Reduced efficacy of chimeric antigen receptor T (CART)-cell therapy is a predominant mechanism of resistance. AXL inhibition can skew CART cells to a Th1 phenotype and can selectively target M2-like cells, leading to improved CART-cell responses in preclinical models.

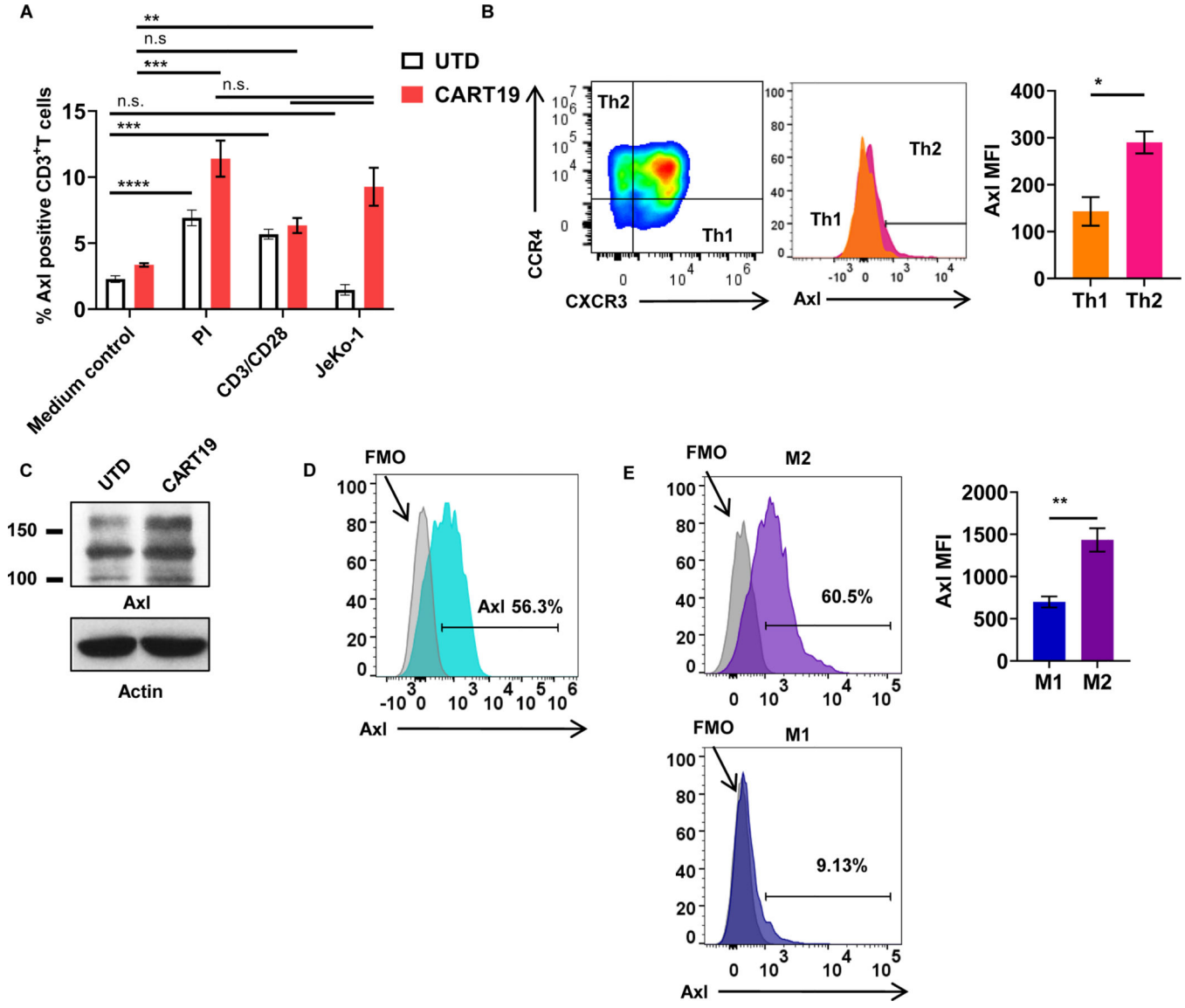

Figure 1: AXL is expressed on activated T cells, CART cells, and innate immune cells.

A, Untransduced T cells (UTDs) or CART19 cells were stimulated with 50 ng/mL PMA and 1.0 μg/mL of ionomycin, $CD3^+CD28^+$ Dynabeads (T cells:beads = 1:3), or $CD19^+$ mantle cell lymphoma cell line, JeKo-1, for 24 hours and assessed for the surface expression of AXL (** $p<0.01$, *** $p<0.001$, **** $p<0.0001$, n.s. not significant, one-way ANOVA). **B**, T cells from experiment Fig.1A were further assessed for helper T-cell (Th) phenotypes. Th1 and Th2 cells were defined by $CD4^+CCR6^-CXCR3^+CCR4^-$ and $CD4^+CCR6^-CXCR3^-CCR4^+$, respectively. AXL expression was assessed by flow cytometry (*** $p<0.0005$, t-test, n=3). **C**, Rested UTD or CART19 cells after their manufacturing were assessed AXL with western blot. **D**, Monocytes were isolated by negative selection using the human classical monocyte isolation kit. Post monocyte isolation, AXL expression was assessed by flow cytometry (n=3). **E**, M1 or M2 induction was performed by the addition of LPS and IFNγ or IL4, respectively. Surface AXL expression of

M1 and M2 macrophages were assessed by flow cytometry (*** $p<0.01$, t-test, n=3). Data are plotted as means ± SEM.

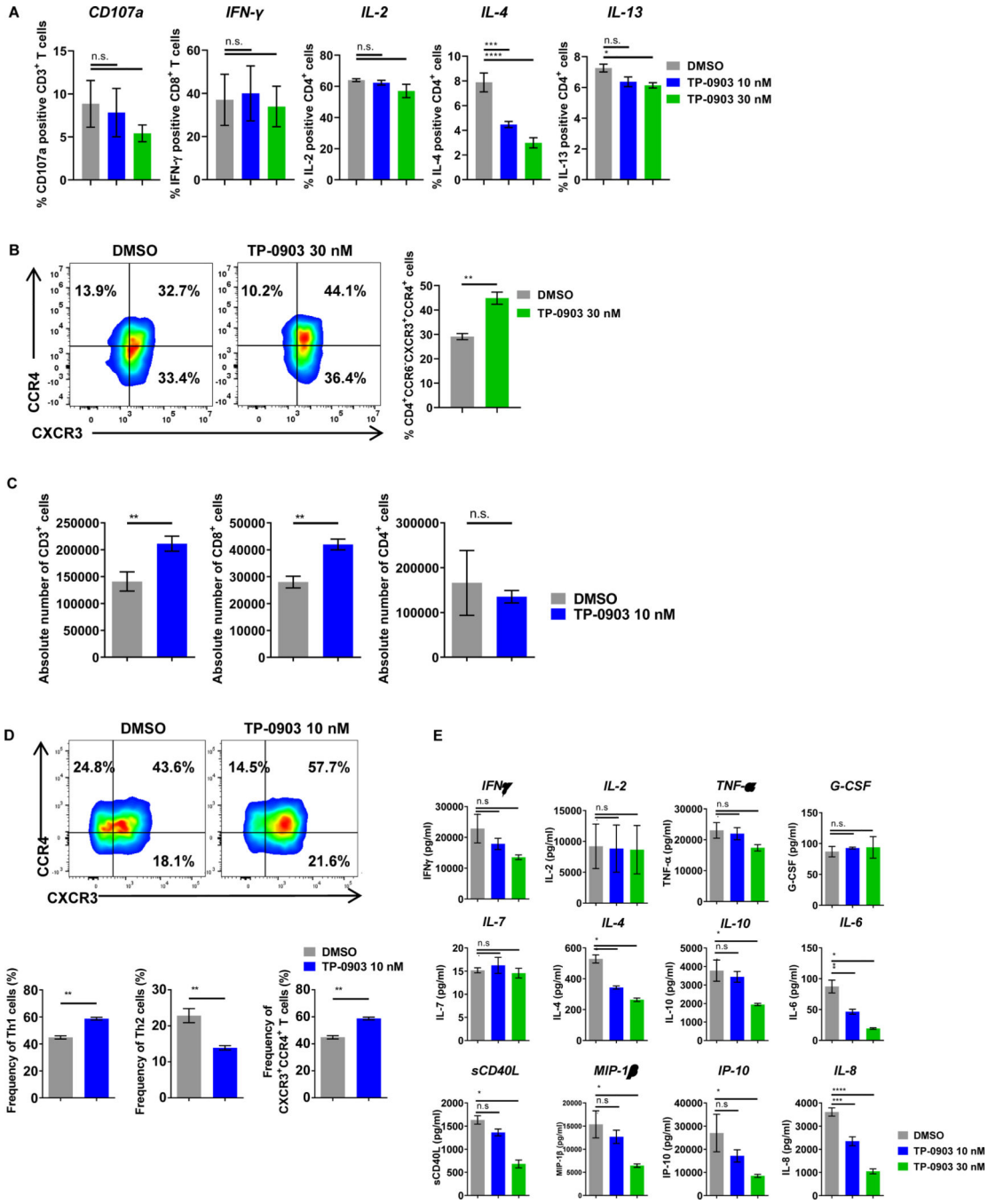

Figure 2: AXL inhibition with TP-0903 selectively reduces Th2 cells and cytokines and enhances CART19-cell proliferation.

A, Naïve T cells were stimulated with 50 ng/mL of PMA and 1 μg/mL of ionomycin for 4 hours in the presence of increasing doses of TP-0903 (10–30 nM). Flow cytometric analysis was used to assess activation of T cells by CD107a degranulation and intracytoplasmic cytokine production (IL2, IFNγ, IL4, IL13). n=3 biological replicates. **B,** Naïve T cells were stimulated with 5 ng/mL of PMA and 0.1 μg/mL of ionomycin for 3 days in the presence of TP-0903 (30 nM). Flow cytometric analysis was used to evaluate $CD4^+CXCR3^+CCR4^+$

T cells (** p<0.01, t-test, n=3 biological replicates). **C,** CART19 cells were co-cultured with the $CD19^+$ mantle cell lymphoma cell line JeKo-1 in the absence or in the presence of TP-0903 (10 nM) for 5 days. CART19 cell proliferation was then assessed for total, $CD8^+$, and $CD4^+$ T cells. n=3 biological replicates. **D,** CART19 cells were co-cultured with JeKo-1 in the presence of TP-0903 (10 nM) for 5 days and chemokine receptors were stained. Th1, Th2, and the $CD4^+CXCR3^+CCR4^+$ fractions were assessed. ** p<0.005, t-test, n=3 biological replicates. **E,** CART19 cells were co-cultured with JeKo-1 cells for 3 days with/without TP-0903, and supernatants were analyzed for human cytokines and chemokines (38-multiplex). * p<0.05, ** p<0.01, *** p<0.001, n=2 biological replicates. Data are plotted as means ± SEM.

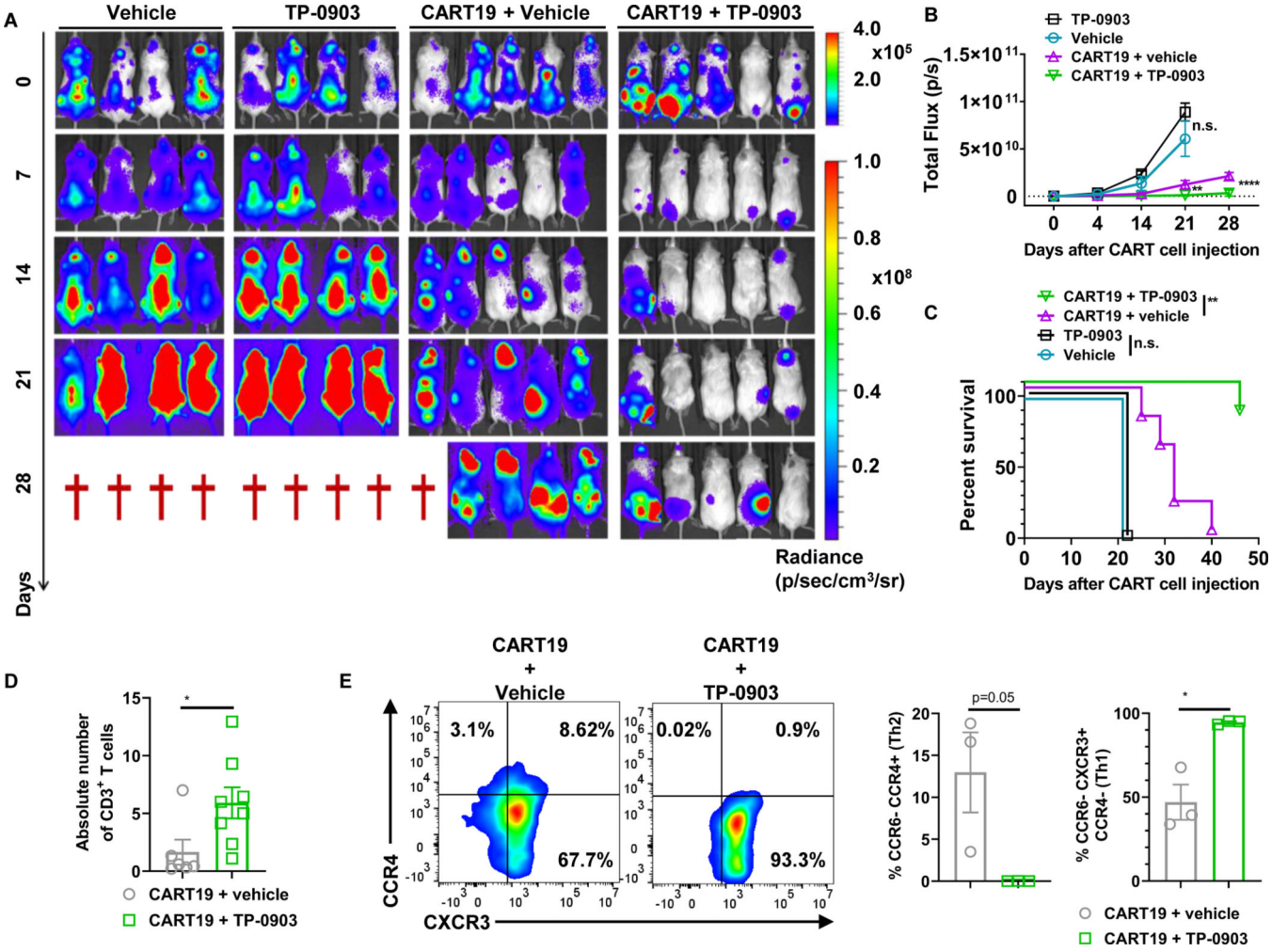

Figure 3: AXL inhibition with TP-0903 enhances CART19 anti-tumor activity *in vivo*.

A, 1.0×10^6 luciferase$^+$ JeKo-1 cells were injected via tail vein into NSG mice. Two weeks after the injection of JeKo-1 tumor burden was analyzed by bioluminescence imaging. Mice were then randomized into groups receiving vehicle (n=4), 20 mg/kg TP-0903 (p.o.) (n=4), 0.5×10^6 of CART19 (i.v.) (n=5), or combination 20 mg/kg TP-0903 and 0.5×10^6 of CART19 (n=5) groups. **B,** Tumor growth based on bioluminescent imaging. ** p<0.005 and **** p<0.0001, two-way ANOVA. **C,** Kaplan-Meier survival curve following different treatments. ** p<0.005, log-rank test, hazard ratio (HR) = 0.089 with 95% confidence interval (CI) (0.01595 to 0.5072), p=0.004. **D**, Mice were bled 17 days after the administration of CART19 cells. Absolute number of CART19 cells was determined via flow cytometry. * p<0.05, t-test, monotherapy group n=6; combination therapy group n=8. **E,** T-cell phenotype after CART19 cell administration was assessed in spleens of a subset of mice. * p<0.05, t-test, both groups n=3.

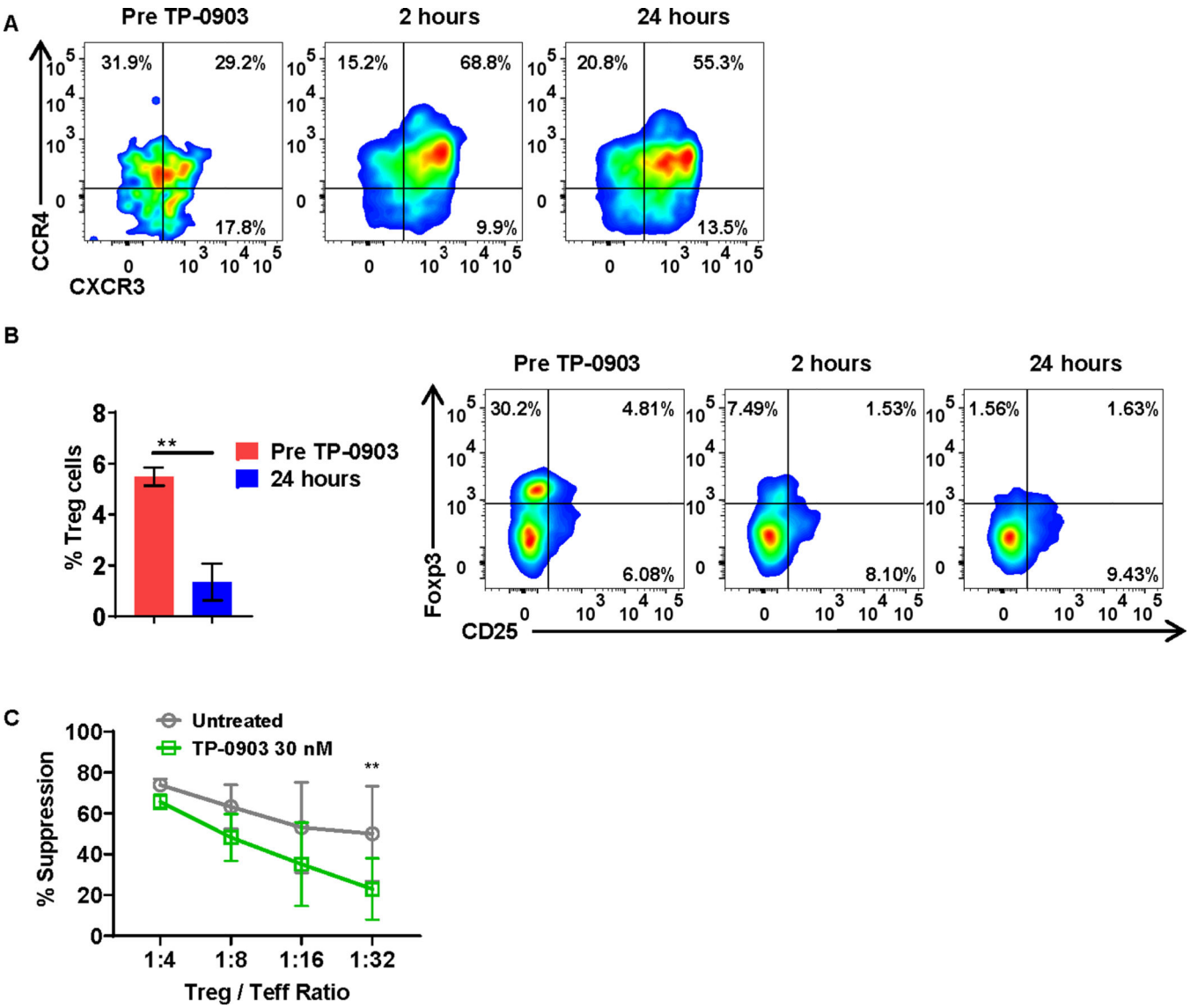

Figure 4: T-cell phenotype is altered following treatment with TP-0903 in a phase I clinical trial for patients with solid tumors (NCT02729298).

A, Peripheral blood-derived Th2 cells ($CD4^+CCR6^-CXCR3^-CCR4^+$) from patients were analyzed before and one day after treatment with TP-0903. Representative flow plot of 3 biological replicates is shown. **B,** Peripheral blood-derived Tregs ($CD4^+CD25^+Foxp3^+$) from patients were analyzed before and one day after treatment with TP-0903. ** $p<0.01$, t-test, n=3 biological replicates. **C**, Tregs and carboxyfluorescein succinimidyl ester (CFSE) stained effector T cell (Teff) cells were co-cultured at the indicated ratio and co-cultured for 4 days in the presence or absence of 30 nM of TP-0903. At the end of the co-culture, the percent suppression of Teff was calculated using flow cytometry. ** $p<0.01$, two-way ANOVA, n=3, biological replicates.

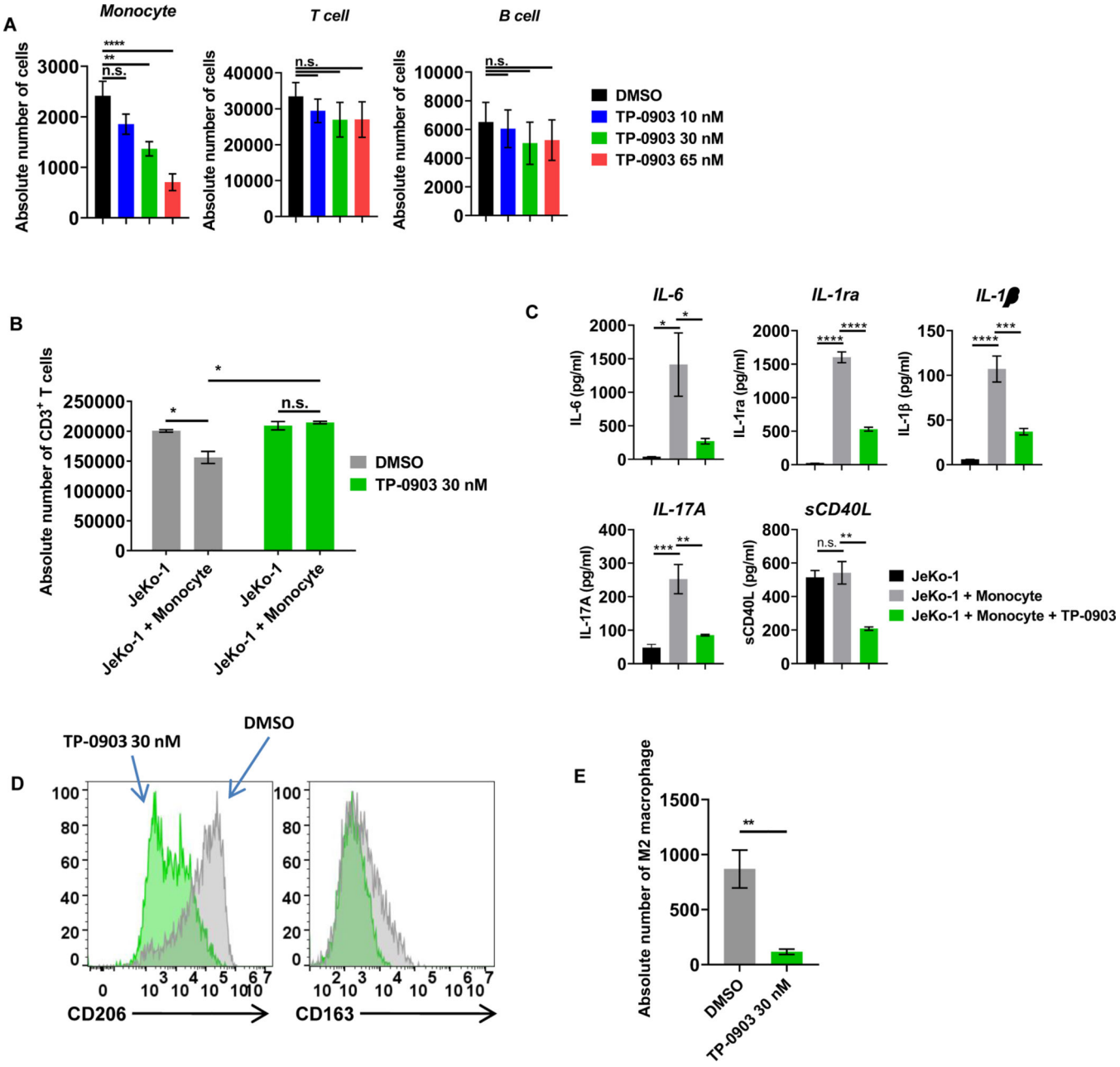

Figure 5: AXL inhibition with TP-0903 preferentially targets monocytes and overcomes monocyte-induced CART-cell suppression.

A, Peripheral blood mononuclear cells derived from healthy donors were treated with increasing doses of TP-0903 (10–65 nM) for 24 hours, and the absolute number of cells was assessed by CountBright bead quantification with flow cytometry (n.s. not significant, ** $p<0.01$, **** $p<0.001$, one-way ANOVA, n=3 biological replicates). **B,** CART19 cells, JeKo-1 cells, and monocytes were co-cultured for 5 days and analyzed for the absolute number of $CD3^+$ T cells by CountBright bead quantification (* $p<0.05$, t-test, n=3 biological replicates). **C,** Supernatants that were harvested from experiment in Fig. 5B were analyzed with 38-mulitplex. (* $p<0.05$, ** $p<0.01$, *** $p<0.001$, **** $p<0.0001$, one-way ANOVA,

n=3 biological replicates). **D,** $CD14^+$ cells were stained for M2-related markers CD206 and CD163 and analyzed via flow cytometry. **E,** CART19 cells, JeKo-1 cells, and M2-like macrophages were co-cultured for 5 days and analyzed for the absolute number of $CD14^+$ cells by flow cytometry (** $p<0.01$, t-test, n=3 biological replicates). Data are plotted as means ± SEM.

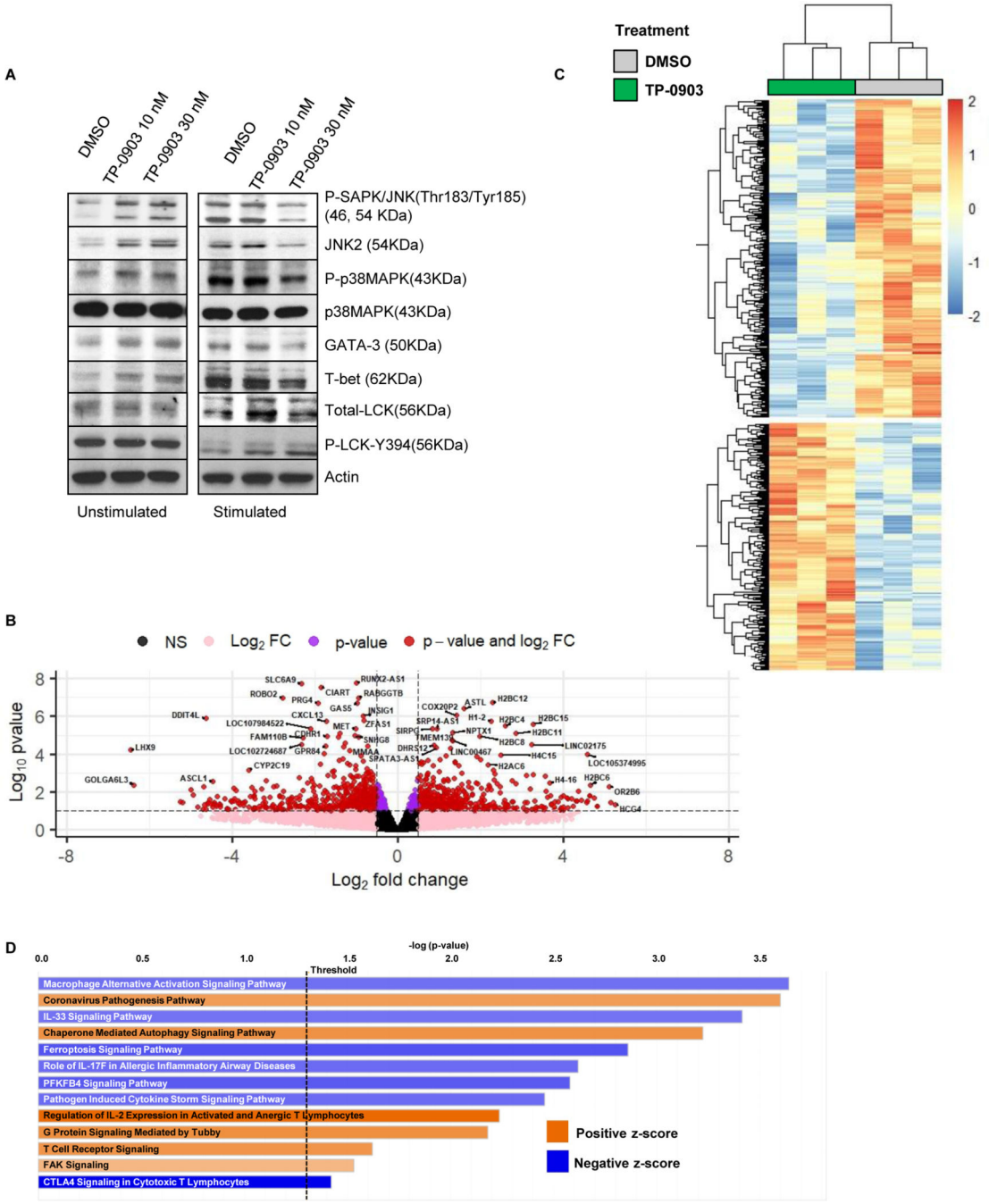

Figure 6: CART19-cell transcriptomic changes following AXL inhibition.

A, CART19 cells were incubated with lethally irradiated JeKo-1 cells in the presence of TP-0903 (10–30 nM) at a 1:3 ratio for 24 hours. After the incubation, T cells were enriched and assessed via western blotting for changes in AXL downstream signaling pathways. **B,** Principal component analysis (PCA) of RNA-seq data from CART19 cells with/without 30 nM of TP-0903. **C-D,** Volcano plot and heatmap showing differential expression of transcripts in TP-0903-treated CART19 cells compared to untreated (DMSO) CART19 cells.

Table 1:

Gene ontology for significantly upregulated genes in CART19 cells treated with TP-0903. Biological processes that overlapped with the significantly differentially upregulated genes between TP-0903-treated or -untreated CART19 cells were identified using Enrichr. The top 5 are listed.

Upstream Regulator	Predicted Activation State	Activation z-score	p-value of overlap
IL4	**Inhibited**	−3.271	9.26E-13
TNF	**Inhibited**	−2.543	1.36E-10
CSF2	**Inhibited**	−2.255	7.83E-10
TGFβ	**Inhibited**	−2.031	7.08E-08
SATB1	n/a	−1.359	2.01E-08